Desalination and Water Treatment
www.deswater.com

doi: 10.1080/19443994.2015.1110720

57 (2016) 20957–20969
September

Taylor & Francis
Taylor & Francis Group

Adsorption of phosphate from municipal effluents using cryptocrystalline magnesite: complementing laboratory results with geochemical modelling

V. Masindi[a,b,*], W.M. Gitari[b], K.G. Pindihama[b]

[a]*CSIR (Council of Scientific and Industrial Research), Built Environment, Hydraulic Infrastructure Engineering, P.O. Box 395, Pretoria 0001, South Africa, Tel. +27 12 841 2787; emails: VMasindi@csir.co.za, masindivhahangwele@gmail.com (V. Masindi)*
[b]*Department of Ecology and Resources Management, School of Environmental Sciences, University of Venda, P/bag X5050, Thohoyandou 0950, South Africa, Tel. +27 15 962 8572; emails: Mugera.gitari@univen.ac.za (W.M. Gitari), gpindihama@gmail.com (K.G. Pindihama)*

Received 14 January 2015; Accepted 16 October 2015

ABSTRACT

The use of low-cost and locally available material in the treatment of wastewater has recently become an issue of interest, and magnesite as a low-cost material has been used for the removal of heavy metals in wastewater and has also shown potential as an adsorbent for the removal of phosphates in wastewater. In this study, batch experiments were conducted to evaluate the effectiveness of cryptocrystalline magnesite in the removal of phosphates from wastewater. Parameters optimized include the following: contact time, dosage, ions concentration and pH. Optimum conditions were observed to be 60 min of agitation, 1 g of dosage, 100 mg L^{-1} ions concentration, 1:100 S/L ratios and pH 10. The phosphate removal efficiency was found to be greater than 99% at an adsorption capacity of 20 mg g^{-1} of magnesite under the optimized conditions. Adsorption kinetics fitted well to pseudo-second-order kinetics than pseudo-first-order kinetics with pore diffusion also acting as a major rate governing step, hence proving chemisorption. Adsorption isotherms fitted well to Langmuir adsorption isotherm than Freundlich adsorption isotherms, demonstrating monolayer adsorption. PHREEQC geochemical model showed $Mg_3(PO_4)_2$ and $MgHPO_4{:}3H_2O$ as the phosphate-bearing mineral phases formed in the removal of phosphate. The optimized method is thus proposed for the application for phosphate removal from wastewater at household and municipal plant levels.

Keywords: Phosphates; Cryptocrystalline magnesite; Isotherms; Kinetics; Geochemical model

1. Introduction

In South Africa, the declining state of municipal wastewater and sewage treatment infrastructure is one of the largest contributing factors to the pollution problems experienced in most parts of the country [1]. A large proportion of the sewage coming from urban areas is not well treated prior to discharge, because the wastewater treatment plants are either incomplete or overloaded [2]. Phosphate is the limiting component for growth in most ecosystems, and discharge of phosphate in surface waters leads to eutrophication and algal bloom, thus having negative impacts on human health and aquatic ecosystems [3–15]. It is thus necessary to control the discharge of phosphates

*Corresponding author.

particularly from wastewater, to meet the limit of 0.5–1.0 mg L^{-1} as required by the South African legislation. Because of the severe environmental problems associated with high levels of phosphates in aquatic ecosystems, there is a need to control the amount of phosphates entering surface waters using chemical or biological techniques.

The usual forms of phosphorus found in aqueous solution include orthophosphate, polyphosphate and organic phosphate with the principal component being orthophosphate and small amounts of organic phosphate [16,17]. Municipal wastewater may contain from 4 to 15 mg L^{-1} phosphorus as phosphate. However, industrial wastewaters (such as detergent manufacturing and metal coating processes) may contain phosphate levels well in excess of 10 mg L^{-1} [1,17–20]. In order to meet effluent quality standards, further treatment of secondary effluent is required. Removal of phosphate from wastewaters has been conducted by adsorption [3,4,21–25], precipitation [3,7,26], reverse osmosis [27], coagulation [28–35], electrochemical [29,36–38], ion exchange [39–44] and phytoremediation [45–51]. The most effective and common methods for phosphate removal are chemical treatment methods including precipitation with calcium [52–55], aluminium [56–60] and iron salts [22,61–63]. However, most of these methods have a high cost of maintenance and are also associated with problems of sludge handling, sludge disposal and neutralization of the effluent [3]. Just like chemical precipitation, adsorption methods have been also been widely used for phosphate removal due to their effectiveness and low costs. The application of low-cost and locally available raw materials in wastewater treatment has recently attracted great interest.

Magnesite is as a low-cost and locally available material and has been used as a potential adsorbent for the removal of heavy metals in wastewater treatment [64–66]. The use of naturally occurring material ensures availability and thus reduces the cost. This study aimed to evaluate and develop a novel technology for the removal of phosphates from municipal wastewaters using the adsorption capacity of cryptocrystalline magnesite.

2. Materials and methods

2.1. Sampling

Raw magnesite rocks were collected from Folovhodwe Magnesite Mine in Limpopo Province, South Africa. The rocks were milled to powder using a Retsch RS 200 miller and passed through a 32-μm particle size sieve. After sieving, the samples were kept in a tightly closed zip-lock plastic bags till required. Municipal wastewater effluent was collected from the Krugersdorp wastewater treatment plant, Gauteng Province, South Africa.

2.2. Chemicals

A known volume of 1,000 mg L^{-1} standard solution of phosphate from Lab Consumables Supply, South Africa, was used as a stock, and dilutions were made accordingly. Milli-Q ultrapure water was used for preparing solutions throughout the study. A known volume of 100 mg L^{-1} solution of phosphate was prepared by extracting 100 mL from the 1,000 mg L^{-1} stock solution, and it was then transferred into a 1,000-mL volumetric flask followed by filling the volumetric flask to the mark by adding ultra-pure water. All reagents used were of analytical grade.

2.3. Characterization

Elemental analysis of raw and processed water samples was done using inductively coupled mass spectrometry (ICP-MS) (ELAN 6000). The chemical characteristics of the magnesite used were determined by X-ray fluorescence spectroscopy (XRF). Mineralogy of the magnesite was determined by X-ray diffraction spectroscopy (XRD). Both XRF and XRD analyses were done at Geology facility of the University of Pretoria. The surface area of the adsorbent was determined by Brunauer–Emmett–Teller (BET). pH_{pzc} was determined using solid addition method [66].

2.4. Batch studies: optimization of adsorption conditions

Optimization experiments were done in batch. Parameters optimized include time, dosage, ions concentration and pH. To determine the effect of agitation time, the time was varied from 1 to 360 min. To evaluate the effects of adsorbent dosage on reaction kinetics, the dosage was varied from 0.1 to 5 g. To evaluate the effect of phosphate concentration, the phosphate ion concentration was varied from 2 to 200 mg L^{-1}. The optimized conditions were then used for further experiments with municipal effluents.

2.5. Modelling

2.5.1. Adsorption kinetics

The effect of contact time on the removal of phosphates from aqueous solution was evaluated using different kinetic models to determine the nature

of the adsorption process and rate-limiting processes. A Lagergren pseudo-first-order kinetic model is a well-known model that is used to describe mechanisms of metal species adsorption by an adsorbent. It can be written as follows [67,68]:

$$\ln\left(q_e - q_t\right) = \ln q_e - k_1 t \tag{1}$$

where k_1 (min^{-1}) is the pseudo-first-order adsorption rate coefficient and q_e and q_t are the values of the amount adsorbed per unit mass at equilibrium and at time t, respectively. The experimental data were fitted using the pseudo-first-order kinetic model by plotting $\ln\left(q_e - q_t\right)$ vs. t. The pseudo-second-order kinetic model is another kinetic model that is widely used to describe the adsorption process from an aqueous solution. The linearized form of the pseudo-second-order rate equation is given as follows:

$$\frac{t}{q_t} = \frac{1}{k_2 q_e^2} + \frac{t}{q_e} \tag{2}$$

where k_2 [g(mg min^{-1})] is the pseudo-second-order adsorption rate coefficient and q_e and q_t are the values of the amount adsorbed per unit mass at equilibrium and at time t, respectively. The overall kinetics of the adsorption from solutions may be governed by the diffusional processes as well as by the kinetics of the surface chemical reaction. In diffusion studies, the rate is often expressed in terms of the square root time:

$$q_t = k_{id} t^{1/2} + C_i \tag{3}$$

where k_{id} (mg g^{-1} $min^{-1/2}$) is the intra-particle diffusion coefficient (slope of the plot of q_t vs. $t^{1/2}$) and C_i is the intra-particle diffusion rate constant.

2.5.2. Adsorption isotherm

The relationship between the amount of ions adsorbed and the concentration of ions remaining in solution is described by an isotherm. The two most common isotherm types for describing this type of system are Langmuir and Freundlich adsorption isotherms. These models describe adsorption processes on a homogenous (monolayer) or heterogeneous (multilayer) surface, respectively. The most important model of monolayer adsorption came from Langmuir. This isotherm is described as follows:

$$q_e = \frac{Q_0 b C_e}{1 + bC_e} \tag{4}$$

The constant Q_0 and b are characteristics of the Langmuir equation and can be determined from a linearized form of equation. The Langmuir isotherm is valid for monolayer sorption due to a surface with finite number of identical sites and can be expressed in the following linear form:

$$\frac{C_e}{q_e} = \frac{1}{Q_m b} + \frac{C_e}{Q_m} \tag{5}$$

where C_e = Equilibrium concentration (mg L^{-1}), Q_e = Amount adsorbed at equilibrium (mg g^{-1}), Q_m = Langmuir constants related to adsorption capacity (mg g^{-1}) and b = Langmuir constants related to energy of adsorption (L mg^{-1}). A plot of $C_e$vs. C_e/Q_e should be linear if the data is described by the Langmuir isotherm. The value of Q_m is determined from the slope and the intercept of the plot. It is used to derive the maximum adsorption capacity and b is determined from the original equation and it represents the intensity of adsorption. The Freundlich adsorption isotherm describes the heterogeneous surface energy by multilayer adsorption. The Freundlich isotherm can be formulated as follows:

$$q_e = k C_e^{1/n} \tag{6}$$

The equation may be linearized by taking the logarithm of both sides of the equation and can be expressed in linear form as follows (Eq. (16)):

$$\log q_e = \frac{1}{n}\log C + \log K \tag{7}$$

where C_e = Equilibrium concentration (mg L^{-1}), q_e = Amount adsorbed at equilibrium (mg g^{-1}), K = Partition Coefficient (mg g^{-1}) and n = Intensity of adsorption. The linear plot of $\log C_e$ vs. $\log q_e$ indicates whether the data is described by Freundlich isotherm. The value of K_f implies that the energy of adsorption on a homogeneous surface is independent of surface coverage and n is an adsorption constant which reveals the rate at which adsorption is taking place. These two constants are determined from the slope and intercept of the plot of each isotherm. An error analysis is required in order to evaluate the fit of the adsorption isotherms to experimental data. In this study, the linear coefficient of determination (R^2) was employed for the error analysis. The linear coefficient of determination is calculated by using the equation:

$$r = \frac{n\sum xy - (\sum x)(\sum y)}{\sqrt{n(\sum x^2) - (\sum x)^2} - \sqrt{(\sum y^2) - (\sum y)^2}} \quad (8)$$

Theoretically, the value of R^2 ranges from 0 to 1. A R^2 value of one shows that 100% of the variation of experimental data is explained by regression equation. The coefficient of determination R^2 was applied to determine the relationship between the experimental data and the isotherms in most studies.

2.6. PHREEQC geochemical modelling

The speciation and mineral phases occurring during the sorption process were predicted using the PHREEQC geochemical modelling code database.

2.7. Treatment of municipal wastewater

A known volume of 100 mL of municipal effluent was transferred into three 250-mL volume HDPE bottles and 1 g of the adsorbent was added. The mixtures were equilibrated for 60 min using a Stuart reciprocating shaker at 250 rpm. After shaking, the mixtures were filtered through 0.45 μm pore cellulose membrane and analysed for the remaining phosphates.

3. Results and discussion

3.1. Characterization of cryptocrystalline magnesite

3.1.1. Elemental composition by XRF

The magnesite consisted of MgO (77%) as the main component with impurities of SiO_2 (5%), CaO (2%), FeO_3 (0.5%) and MnO (5%). After contacting magnesite with phosphate-rich water, the levels of phosphates (5%) were observed to be available in the secondary residues, hence indicating that magnesite is scavenging phosphates from wastewater. This has corroborated the XRD results which indicated the presence of magnesite and quartz in the magnesite soils.

3.1.2. Mineralogical composition by XRD

The mineralogical composition of the cryptocrystalline magnesite is presented in Fig. 1.

As shown in Fig. 1, cryptocrystalline magnesite contains magnesite and quartz. This indicates that the material used was predominantly cryptocrystalline

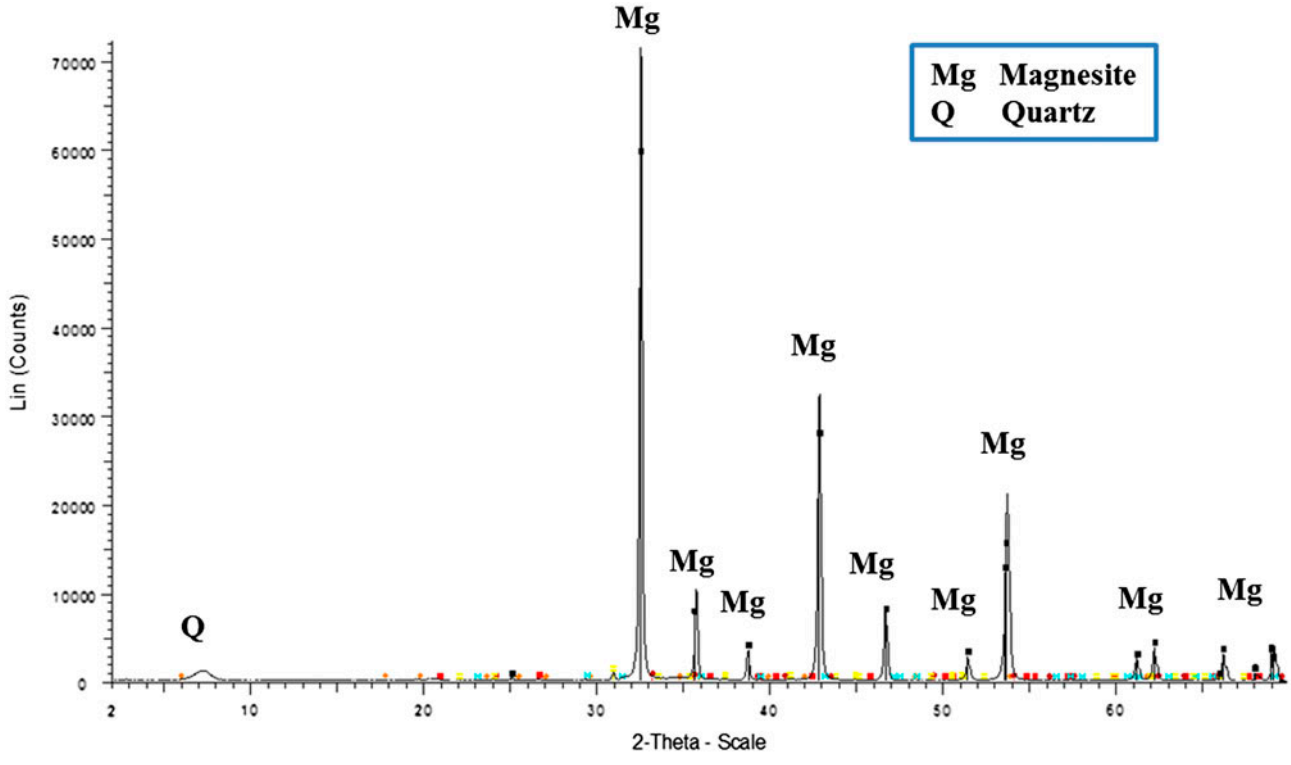

Fig. 1. Mineralogical composition of cryptocrystalline magnesite.

Table 1
Surface properties and pH_{PZC} of cryptocrystalline magnesite

Parameter	Magnesite
BET surface area	14.6129
Micropore area	2.271
External surface area	12.3419
Micropore volume	0.0009
Adsorption average pore diameter (4 V/A by BET)	222.9594
Point of zero charge (pH_{PZC})	12

magnesite with few impurities of quartz. Based on the XRD results, the precipitation reaction between phosphate and magnesite could be described as follows:

$$Mg^{2+} + H^{+} + PO_4^{3-} + 2H_2O = MgHPO_4 \cdot 2H_2O \quad (9)$$

3.1.3. Surface area and point of zero charge (pH_{PZC})

The results for surface area and pH_{PZC} for magnesite are shown in Table 1

Surface area is one of the most important aspects in the adsorption process. High surface area attributes to high adsorption capacity of the material since more surfaces are available for adsorption [18–20,69–72]. The magnesite was found to have a surface area of 14.6 m^2/g. The surface area is a combination of external surface area and micropore area. The point of zero charge (pH_{pzc}) is one of the important parameters in adsorption since it dictates the type of species that will be adsorbed by the material at a given pH. Simply put, when the pH of a solution is greater than pH_{pzc}, the material will adsorb cations, and when the pH of the solution is less than the pH_{pzc}, the material will adsorb anions [16]. The cryptocrystalline magnesite was found to have a pH_{pzc} of 12. This corresponded with results in other studies [16] which also found the pH_{pzc} of MgO to be 12.4. As such, at pH lower than 12, the phosphate is much likely to be adsorbed by the cryptocrystalline magnesite in aqueous solution.

3.2. Batch experiments: Optimization of phosphate removal conditions

Effect of contact time, adsorbent dosage, phosphates concentration and pH on the removal of phosphate species from aqueous solution was evaluated in batch experimental procedures.

3.2.1. Effect of shaking time on the removal of phosphate

Effect of shaking time on the removal of phosphate from aqueous solution is shown in Fig. 2.

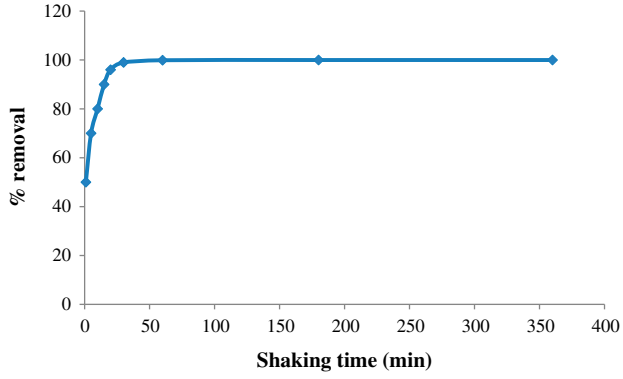

Fig. 2. Variation of phosphate removal with shaking time (Conditions: 1 g dosage, 100 mg L^{-1} phosphate concentration, pH < 7, 250 rpm shaking speed, 1:100 S/L ratios, 100 mL and 26°C).

The percentage removal of phosphates was monitored with an increase in shaking time and (Fig. 2). The removal of phosphates by magnesite increased with an increase in shaking time. The uptake was observed to be rapid from the 1st minute of contact leading to >50% removal efficiency. After 60 min of shaking, approximately 100% removal efficiency was achieved, and thereafter, no significant uptake was observed, hence indicating that the reaction had reached equilibrium. From the first few minutes to 60 min, the removal efficiency increased from approximately 50–100%; thus, a shaking time of 60 min was found to be the optimum time for the subsequent experiments.

3.2.2. Effect of adsorbent dosage on removal of phosphate

The effect of the adsorbent dosage on the removal of phosphates from aqueous solution is shown in Fig. 3.

The effect of magnesite dosage on the removal of phosphates from aqueous solutions was evaluated by varying the adsorbent dosage from 0 to 5 g per 100 mL of the solution. A known volume of 100 mL of

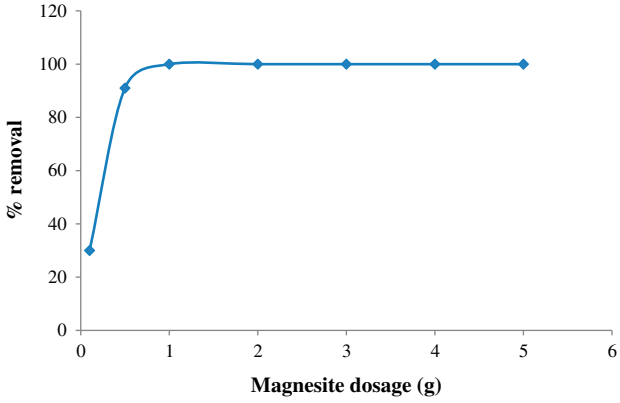

Fig. 3. Variation of phosphate removal with adsorbent dosage (Conditions: 60 min of shaking time, 100 mg L^{-1} phosphate concentration, pH < 7, 250 rpm shaking speed, 100 mL aqueous solution and 26˚C).

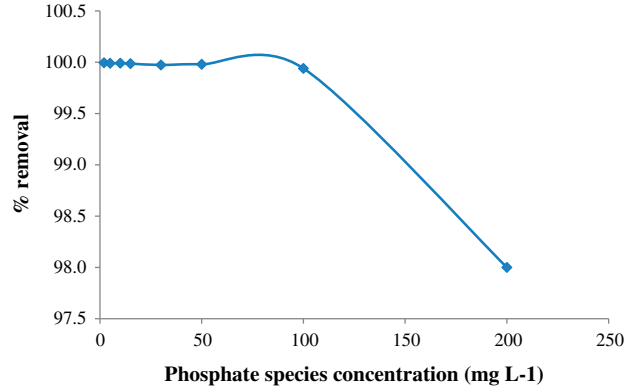

Fig. 4. Variation of phosphate removal with varying phosphate species concentration (Conditions: 60 min of shaking time, 1 g dosage, 1:100 S/L ratios, pH < 7, 250 rpm shaking speed, 100 mL aqueous solution and 26˚C).

aqueous solution was pipetted into 250 mL of high-density polyethylene (HDPE) plastic bottles. Varying dosages (1–5 g/100 mL) of magnesite were added. The percentage removal of phosphates was monitored with increasing magnesite dosage. Removal of phosphates by magnesite increased with an increase in magnesite dosage (Fig. 3). The uptake of phosphates was observed to increase as the adsorbent dosage was increasing from 0.1 to 1 g. This can simply be explained by the mere fact that the increase in the adsorbent dose led to a greater surface area. At low dosages, there are finite surfaces available for the adsorption to take place, and at higher dosages, more surfaces are available. From 0.1 to 1 g, the removal efficiency increased from approximately 30–100%, and thereafter, an increase in the adsorbent dose did not have any significant impact on the uptake. At a higher dosage, the equilibrium uptake of phosphate ions did not increase significantly with increasing magnesite dosage. This is because, at high dosages (beyond 1 g/100 ml), the saturation level would have been attained during an adsorption process. Therefore, 1 g was taken as the optimum dosage for the subsequent experiments.

3.2.3. Effect of phosphate concentration on the adsorption process

The effect of phosphate species concentration on the adsorption process in aqueous solution is shown in Fig. 4.

The effect of phosphate removal as a function of species concentration was evaluated from 2 to 200 mg L^{-1} phosphate concentration. As shown in Fig. 4, there was a decrease in % removal of phosphate with an increase in phosphate concentration. It can be clearly seen in Fig. 4 that as the concentration of phosphate ions was increased beyond 100 mg L^{-1}, the % removal rapidly decreased. At low concentration, more surfaces are available for the sorption to take place, and at high concentrations, fewer surfaces are available for the adsorption. From 2 to 100 mg L^{-1}, approximately 100% of phosphate removal was achieved, and thereafter, the uptake reduced, indicating that the vacant surfaces were all occupied with phosphates. High adsorption of phosphate at low concentration is attributed to large number of vacant sites available on the adsorbent. As the concentration increased, more surfaces were being occupied by the phosphate ions in solution, hence making the available surfaces to be reduced. Over the concentration range of 2–100 mg L^{-1}, magnesite managed to remove ≈100% of phosphates in aqueous solution. This demonstrated that the magnesite used had a strong affinity for phosphates. It was thus concluded that 60 min of contact time, 1 g of dosage and a 100 mg L^{-1} concentration of phosphate ions were the optimum conditions for the adsorption of phosphates by magnesite in aqueous solution.

3.2.4. Effect of supernatants pH

The effect of pH on the adsorption of phosphate ions by magnesite in aqueous solution is shown in Fig. 5.

The effect of pH on the removal of phosphates from aqueous solution was evaluated at pH ranging from 2 to 12. Hundered milliliters of aqueous solution with phosphate being pipetted into 250 mL of HDPE plastic

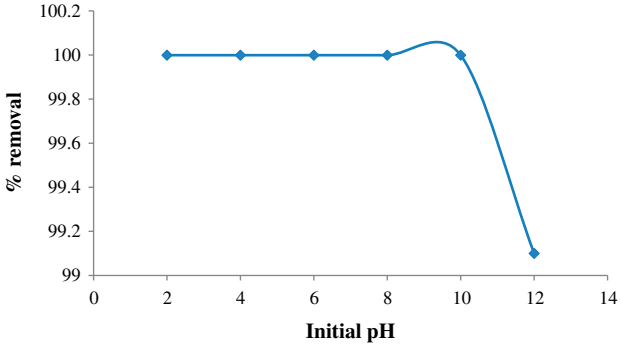

Fig. 5. Percentage phosphate removal with varying pH levels (Conditions: 60 min of shaking time, 1 g dosage, 1:100 S/L ratios, 100 mg L^{-1} phosphate concentration, 250 rpm shaking speed, 100 mL aqueous solution and 26°C).

bottles and 1 g of magnesite added. The mixture was equilibrated for 60 min. The percentage removal of phosphates was monitored at various pH. Removal of phosphates by magnesite at varying pH was observed to be high over a wide range of pH (Fig. 4). From pH 2 to 12, the removal efficiency was greater than 98%. The pH-dependent increase is due to increasing adsorption of formed phosphate anions, with pK_a 7.2, and with the positively charged surface sites of the magnesite. High adsorption of magnesite may also be attributed to the high pH_{pzc} magnesite which was found to be around 12 (Table 2). As such at pH < 12, magnesite has a high affinity for anions like phosphate in aqueous solution, and at pH > 12, adsorption of anions is poor (Fig. 5). As such, pHs of 2–10 were observed to be suitable for the subsequent experiments.

3.3. Adsorption kinetics and mechanisms

In general, kinetic studies provide information on the amount of adsorbate being adsorbed over time, which later reflects the residence time to complete the reaction. Mechanisms involved during the reaction of magnesite and phosphate were determined using adsorption kinetics. The commonly used kinetics is pseudo-first-order and pseudo-second-order kinetics. Fig. 6 shows pseudo-first-order and pseudo-second-order kinetics.

As shown in Table 4, the kinetic data fitted better to pseudo-second-order adsorption isotherm than pseudo-first-order kinetic model and intra-particle diffusion model, hence confirming chemisorption. The experimental adsorption capacity was comparable to the calculated adsorption capacity, hence further confirming better fit of pseudo-second order. Magnesite is porous as proved by BET (Table 1). Diffusion of solute filling the pores could influence the rate of adsorption. To explain the mechanism of intra-particle diffusion, the Weber–Morris model is used to illustrate the concept. Interaction of solute with the adsorbent can be defined by four major steps: Bulk diffusion, film diffusion, pore diffusion and adsorption at active sites (Fig. 7) [73].

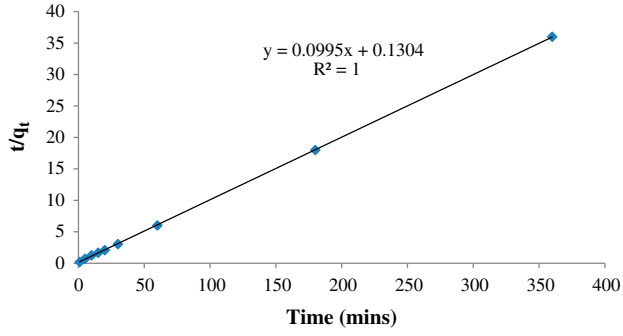

Fig. 6. Pseudo-second-order plot for phosphate adsorption by cryptocrystalline magnesite.

Table 2
Different kinetic model parameters for adsorption of phosphate by cryptocrystalline magnesite

Element	R^2	k_1 (min^{-1})	$q_{e(cal)}$ (mg g^{-1})	$q_{e(exp)}$ (mg g^{-1})
Pseudo-first-order kinetics				
Phosphate	0.2	0.06	–2,500	10
Pseudo-second-order kinetics				
Element	R^2	k_2 (g mg min^{-1})	$q_{e(cal)}$ (mg g^{-1})	$q_{e(exp)}$ (mg g^{-1})
Phosphate	1	0.9	10	10
Intra-particle-diffusion model				
Element	R^2	C_i (mg g^{-1})	k_{id} (mg g^{-1} $min^{-1/2}$)	$q_{e(exp)}$ (mg g^{-1})
Phosphate	0.4	7.4	0.2	10

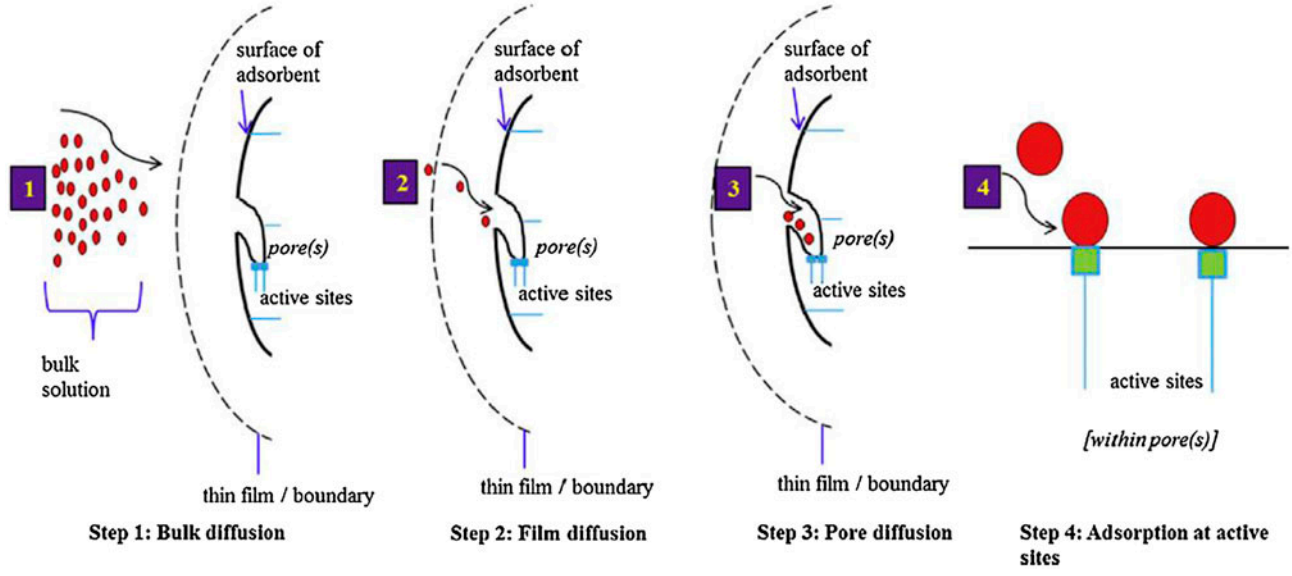

Fig. 7. Proposed diagram for the transportation of solute to adsorbent (not to scale).

The plot of $t^{0.5}$ and q_t (mg g^{-1}) by Webber–Morris model indicated that there are more than one rate-limiting step that are involved when an adsorbate is being removed from aqueous solution. The first step is a very steep slope which represents-film diffusion (2), and the second step which is slightly steep slope represents pore diffusion (3), and the final step of linearity indicates that the reaction has approached the equilibrium phase. The linear plots did not pass through the origin, hence indicating that intra-particle diffusion is not the only step governing the chemical reaction (Fig. 8). The lower K_{id} (mg g^{-1}min$^{-1/2}$) indicates that the adsorption process is taking place at a very fast rate with high adsorption capacity as represented by high C_i (mg g^{-1}) (Table 2) which is pretty much close to the experimental value.

3.4. Adsorption isotherms

Equilibrium data are basic requirements for the design of adsorption systems and are used for the mathematical description of the adsorption equilibrium of the metal ion on the adsorbent. Data for the adsorption of phosphate ions by magnesite were analysed by Langmuir and Freundlich adsorption isotherms. The sorption data for the removal of phosphate ion was correlated with the Langmuir and Freundlich adsorption models, Figs. 9 and 10, respectively.

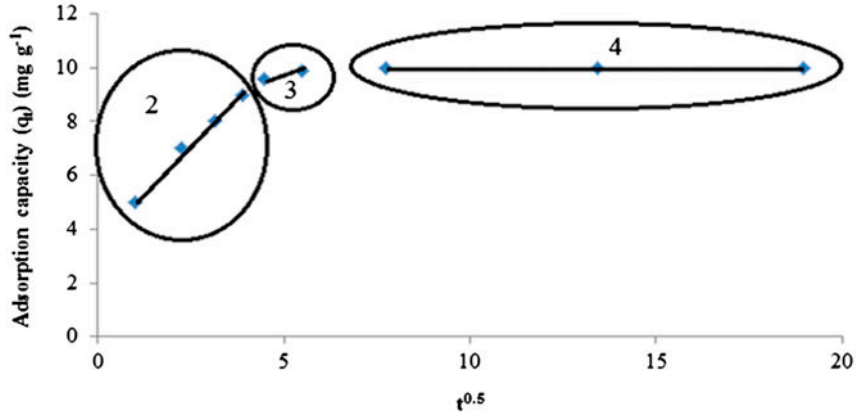

Fig. 8. Intra-particle diffusion plots for phosphate by cryptocrystalline magnesite.

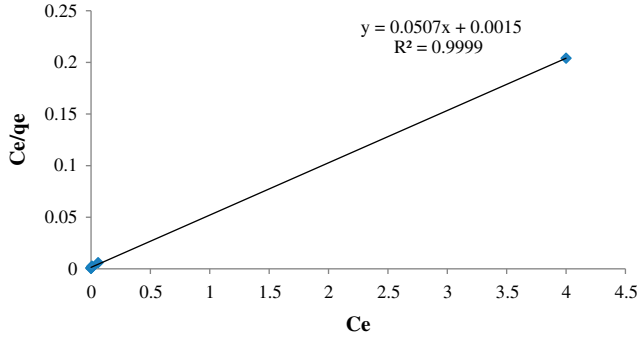

Fig. 9. Langmuir adsorption plot for phosphate.

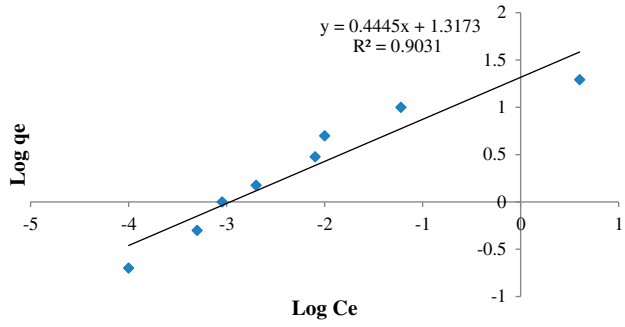

Fig. 10. Freundlich adsorption plot for phosphate.

The parameters of Langmuir and Freundlich adsorption isotherms are shown in Table 3.

As tabulated, the Langmuir showed high correlation coefficient ($R^2 > 0.99$) (Fig. 9). The "Q_m" and "b" show that the adsorption of phosphate by magnesite takes place at high energy with high intensity of adsorption. The Freundlich adsorption isotherm also showed a good regression coefficient ($R^2 > 0.90$) (Fig. 10). The n value between 1 and 10 shows the feasibility of the reaction with high adsorption capacity as indicated by high K_f value. This indicates a good agreement between the experimental values 20 mg g^{-1} and isotherm parameters. The data fitted well to Langmuir adsorption isotherm than Freundlich adsorption isotherm, hence showing that phosphate adsorption by magnesite depicts a monolayer adsorption mode.

3.5. Geochemical modelling

PHREEQC geochemical modelling code was used to determine the saturation indices of the main phosphate mineral phases during the adsorption process. PHREEQC geochemical model predicted that the phosphate-bearing mineral phases were $Mg_3(PO_4)_2$ and $MgHPO_4{:}3H_2O$. Moreover, it was postulated that monodentate or bidentate inner sphere surface complex between phosphate (P–OH) and hydroxyl group on alkali metal (Mg–OH) might be formed during the chemical reaction. According to Fig. 11, it could be seen that there was electrostatic attraction between negatively charged phosphate species (HPO_4^{2-} and $H_2PO_4^-$) and electropositive adsorbent surface since the pH of the solution was below pH_{pzc} of the adsorbent. So the possible adsorption reaction between the aqueous phosphate and magnesite could be better described by Fig. 11.

3.6. Comparison of adsorption capacity of magnesite with other adsorbents

Table 4 shows a comparison of the adsorption capacity of cryptocrystalline magnesite against other adsorbents used for phosphate removal.

Sorption capacity of cryptocrystalline magnesite for phosphate has shown better sorption capacity as compared to other studies except for activated MgO, magnesite-bentonite clay composite and Ferric sludge. The above data prove that magnesite can be used as a substitute for conventional adsorbents, but issues such as cost, availability and feasibility will need further investigation.

Table 3
Langmuir and Freundlich parameters

	Langmuir adsorption isotherm			
Chemical species	R^2	Q_m (mg g^{-1})	$q_{e(exp)}$ (mg g^{-1})	b (L mg^{-1})
Phosphate	0.99	19.7	20	33.3
	Freundlich adsorption isotherm			
Chemical species	R^2	k_f (mg g^{-1})	$q_{e(exp)}$ (mg g^{-1})	n
Phosphate	0.9	20.8	20	2.2

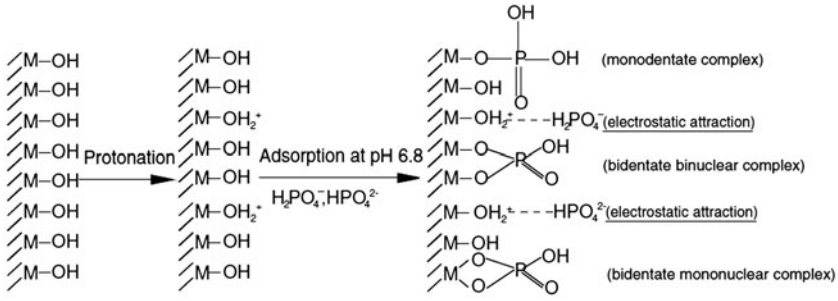

Fig. 11. Schematic presentation of possible phosphate adsorption reaction.

Table 4
Adsorption capacity of adsorbents for phosphate

Feedstock	Adsorption capacity (mg g^{-1})	Refs.
Cryptocrystalline magnesite	20	Present study
Magnesite/bentonite clay composite	82	[66]
Hydrous Niobium oxide	15.0	[74]
Magnetite Iron oxide nanoparticles	0.33	[75]
Paper mill sludge	12	[76]
Activated MgO	95.2	[77]
Ferric sludge	25.5	[78]
Oyster shell	0.7	[79]
Bauxite	3.0	[80]

3.7. Treatment of municipal wastewater under optimized conditions

Chemical composition of treated and raw municipal effluents is shown in Table 5.

The raw municipal effluent used obviously contained a host of other anions and cations, a few of which were analysed in this study and are presented in Table 5. After treatment, the levels of most of the other cations which were analysed together with phosphate were observed have significantly decreased after the treatment. The findings demonstrated that magnesite can take up phosphates and host of other anions and metals in municipal effluents. The presence of anions such as chloride and bromide were observed not to affect the adsorption of phosphate by magnesite. A significant amount of nitrate was also removed from municipal effluent.

Table 5
Composition of raw and treated municipal effluents

Parameter	Before treatment	After treatment
pH	5	10
EC (μS/cm)	123	40
TDS (g/L)	61	19
NO_3^- (mg/L)	100	50
PO_4^{3-} (mg/L)	90	0.1
Chloride	80	75
Bromide	15	10
Ni (mg/L)	2.5	0.001
Cu (mg/L)	7	0.001
Zn (mg/L)	1	0.001
Pb (mg/L)	9	0.001

4. Conclusions

After the batch experiments, the following conclusions were drawn:

(1) Cryptocrystalline magnesite successfully removed phosphates from municipal wastewater effluents.
(2) Optimum conditions for the removal of phosphates were observed to be 60 min, 1 g, 100 mg L^{-1}, pH 10, 1:100 S/L ratios and 250 rpm.
(3) Greater than 99% removal efficiency and 20 mg g^{-1} were reported under the optimized conditions.
(4) Adsorption kinetics fitted well to pseudo-first order than pseudo-second order with pore diffusion as the major step determining the chemical reaction, hence confirming chemisorption.

(5) Adsorption data fitted well to Langmuir adsorption isotherm than Freundlich adsorption isotherm, hence proving monolayer adsorption.
(6) The raw, unprocessed and locally available cryptocrystalline magnesite has good adsorption capacity as compared to other conventional adsorption methods previously studied.
(7) PHREEQC geochemical model predicted that phosphates precipitate as $Mg_3(PO_4)_2$ and $MgHPO_4{:}3H_2O$ from aqueous solution.

Acknowledgements

The authors wish to express their sincere gratitude to the Council of Scientific and Industrial research (CSIR), Environmental Remediation and Water Pollution Chemistry Research Group, University of Venda Directorate, Department of Ecology and Resource Management, ESKOM-TESP, SASOL-Inzalo and DST-NRF for supporting this project financially.

References

[1] V. Masindi, W. Gitari, H. Tutu, Assessment of the Impact of Upstream Agricultural Activities on the Quality of the River Water Around Damani Dam, South Africa, University of Venda Publishers, South Africa, Limpopo Province, 2011.
[2] S. Tillotson, Phosphate removal: An alternative to chemical dosing, Filtr. Sep. 43 (2006) 10–12.
[3] M. Zulfiqar, A.A. Omar, S. Chowdhury, Removal of phosphate and fluoride from industrial wastewater—A short review, Appl. Mech. Mater. 625 (2014) 805–808.
[4] X. Zhu, H. Liu, P. Shi, J. Wu, Y. Guo, Removal of phosphate from aqueous solution by using red mud, Adv. Mater. Res. 291–294 (2011) 1804–1807.
[5] Y. Zhao, J. Wang, Z. Luan, X. Peng, Z. Liang, L. Shi, Removal of phosphate from aqueous solution by red mud using a factorial design, J. Hazard. Mater. 165 (2009) 1193–1199.
[6] L. Zhang, L. Wan, N. Chang, J. Liu, C. Duan, Q. Zhou, X. Li, X. Wang, Removal of phosphate from water by activated carbon fiber loaded with lanthanum oxide, J. Hazard. Mater. 190 (2011) 848–855.
[7] G. Zhang, H. Liu, R. Liu, J. Qu, Removal of phosphate from water by a Fe-Mn binary oxide adsorbent, J. Colloid Interface Sci. 335 (2009) 168–174.
[8] F. Zhang, H. Zhang, L. Zhang, The removal of phosphate by coal gangue from wastewater, Appl. Mech. Mater. 209–211 (2012) 2005–2008.
[9] M. Zamparas, A. Gianni, P. Stathi, Y. Deligiannakis, I. Zacharias, Removal of phosphate from natural waters using innovative modified bentonites, Appl. Clay Sci. 62–63 (2012) 101–106.
[10] X.L. Yuan, W.T. Xia, J. An, W.Q. Yang, J.G. Yin, Removal of phosphate anions from aqueous solutions using dolomite as adsorbent, Adv. Mater. Res. 55 (2014) 1454–1457.
[11] Y. Yang, Y.Q. Zhao, A.O. Babatunde, L. Wang, Y.X. Ren, Y. Han, Characteristics and mechanisms of phosphate adsorption on dewatered alum sludge, Sep. Purif. Technol. 51 (2006) 193–200.
[12] Y. Zhang, B. Pan, Modeling batch and column phosphate removal by hydrated ferric oxide-based nanocomposite using response surface methodology and artificial neural network, Chem. Eng. J. 249 (2014) 111–120.
[13] Y. Wu, Y. Yu, J.Z. Zhou, J. Liu, Y. Chi, Z.P. Xu, G. Qian, Effective removal of pyrophosphate by Ca-Fe-LDH and its mechanism, Chem. Eng. J. 179 (2012) 72–79.
[14] A. Abeynaike, L. Wang, M.I. Jones, D.A. Patterson, Pyrolysed powdered mussel shells for eutrophication control: Effect of particle size and powder concentration on the mechanism and extent of phosphate removal, Asia-Pac. J. Chem. Eng. 6 (2011) 231–243.
[15] L.L. Wang, Y.B. Huang, H. Hu, C.Y. Hong, Q. Huang, J. Dong, S.X. Tu, W.Q. Gong, Y. Li, Adsorption of phosphate onto natural manganese ore, Wuhan Ligong Daxue Xuebao/J. Wuhan Univ. Technol. 34 (2012) 76–80.
[16] D.L. Sparks, Environmental Soil Chemistry, Academic Press, San Diego, CA, 1995.
[17] I.L. Pepper, C.P. Gerba, M.L. Brusseau, Environmental and Pollution Science, Elsevier Science, San Diego, CA, 2011.
[18] M.A. Vicente, A. Gil, F. Bergaya, Chapter 10.5—Pillared Clays and Clay Minerals, in: B. Faïza, L. Gerhard (Eds.) Developments in Clay Science, Elsevier, Amsterdam, 2013, pp. 523–557.
[19] R.M. Harrison, Introduction to Pollution Science, RSC Publishing, San Diego, CA, 2006.
[20] B.J. Alloway, Heavy Metals in Soils, Chapman & Hall, San Diego, CA, 1990.
[21] E.M. Zong, D. Wei, Z.K. Huan, D. Peng, H.Q. Wan, S.R. Zheng, Z.Y. Xu, Adsorption of phosphate by zirconia functionalized multi-walled carbon nanotubes, Chin. J. Inorg. Chem. 29 (2013) 965–972.
[22] M.X. Zhu, K.Y. Ding, S.H. Xu, X. Jiang, Adsorption of phosphate on hydroxyaluminum- and hydroxyiron-montmorillonite complexes, J. Hazard. Mater. 165 (2009) 645–651.
[23] J. Zhang, Z. Shen, W. Shan, Z. Chen, Z. Mei, Y. Lei, W. Wang, Adsorption behavior of phosphate on Lanthanum(III) doped mesoporous silicates material, J. Environ. Sci. 22 (2010) 507–511.
[24] H. Zhang, L. Zhang, W. Guo, W. Wu, M. Zhang, L. Han, Phosphate removal potential of applying red mud derived from bauxite calcination method for water cleanup, Fresenius Environ. Bull. 21 (2012) 1539–1547.
[25] L. Zeng, X. Li, J. Liu, Adsorptive removal of phosphate from aqueous solutions using iron oxide tailings, Water Res. 38 (2004) 1318–1326.
[26] Y. Yang, Y.M. Zhang, J.J. Lian, J.C. Duan, C. Zhou, C. Lin, Preparation and adsorptive properties of carbonized rice straw based phosphate sorbent, J. Ecol. Rural Environ. 29 (2013) 755–761.
[27] D. Dolar, K. Košutić, B. Vučić, RO/NF treatment of wastewater from fertilizer factory—Removal of fluoride and phosphate, Desalination 265 (2011) 237–241.

[28] Y. Zhao, L.-Y. Zhang, F. Ni, B. Xi, X. Xia, X. Peng, Z. Luan, Evaluation of a novel composite inorganic coagulant prepared by red mud for phosphate removal, Desalination 273 (2011) 414–420.
[29] S. Zhang, J. Zhang, W. Wang, F. Li, X. Cheng, Removal of phosphate from landscape water using an electrocoagulation process powered directly by photovoltaic solar modules, Sol. Energy Mater. Sol. Cells 117 (2013) 73–80.
[30] L.H. Sun, T.M. Yu, X.R. Chen, X.L. Qi, Y.J. Zhang, Influencing factors of the *in situ* formed iron hydroxide (FeOxHy) on the removal of phosphate by coagulation and adsorption, Adv. Mater. Res. 864–867 (2014) 1772–1778.
[31] L.H. Sun, X.L. Qi, Y.J. Zhang, Effectiveness and mechanism of the *in situ* formed iron hydroxide (FeOxHy) towards the removal of phosphate by coagulation and adsorption, Adv. Mater. Res. 807–809 (2013) 1251–1257.
[32] X. Qi, L. Sun, Y. Zhang, B. Liu, Effectiveness and mechanism of the *in situ* formed iron hydroxide (FeOxHy) towards the removal of phosphate by coagulation and adsorption, Chin. J. Environ. Eng. 8 (2014) 505–512.
[33] H. Inan, E. Alaydın, Phosphate and nitrogen removal by iron produced in electrocoagulation reactor, Desalin. Water Treat. 52 (2014) 1396–1403.
[34] Y. Wang, J. Tan, J. Liu, Y. Chen, X. Li, Removal of template from mesostructured nickel phosphates by solvent extraction, Acta Chim. Sinica 68 (2010) 2471–2476.
[35] A. Attour, M. Touati, M. Tlili, M. Ben Amor, Influence of operating parameters on phosphate removal from water by electrocoagulation using aluminum electrodes, Sep. Purif. Technol. 123 (2014) 124–129.
[36] S. Yang, Y. Zhao, D. Ding, Y. Wang, C. Feng, Z. Lei, Y. Yang, Z. Zhang, An electrochemically modified novel tablet porous material developed as adsorbent for phosphate removal from aqueous solution, Chem. Eng. J. 220 (2013) 367–374.
[37] J. Yang, Q. Zeng, L. Peng, M. Lei, H. Song, B. Tie, J. Gu, La-EDTA coated Fe_3O_4 nanomaterial: Preparation and application in removal of phosphate from water, J. Environ. Sci. 25 (2013) 413–418.
[38] M.I. Tejedor-Tejedor, M.A. Anderson, The protonation of phosphate on the surface of goethite as studied by CIR-FTIR and electrophoretic mobility, Langmuir 6 (1990) 602–611.
[39] H. Yin, M. Kong, Simultaneous removal of ammonium and phosphate from eutrophic waters using natural calcium-rich attapulgite-based versatile adsorbent, Desalination 351 (2014) 128–137.
[40] X. Xu, B.Y. Gao, Q.Y. Yue, Q.Q. Zhong, X. Zhan, Preparation, characterization of wheat residue based anion exchangers and its utilization for the phosphate removal from aqueous solution, Carbohydr. Polym. 82 (2010) 1212–1218.
[41] X. Xu, B.Y. Gao, Q.Y. Yue, Q.Q. Zhong, Preparation of agricultural by-product based anion exchanger and its utilization for nitrate and phosphate removal, Bioresour. Technol. 101 (2010) 8558–8564.
[42] A. Sowmya, S. Meenakshi, A novel quaternized chitosan–melamine–glutaraldehyde resin for the removal of nitrate and phosphate anions, Int. J. Biol. Macromol. 64 (2014) 224–232.
[43] A. Sowmya, S. Meenakshi, Removal of nitrate and phosphate anions from aqueous solutions using strong base anion exchange resin, Desalin. Water Treat. 51 (2013) 7145–7156.
[44] T. Nur, M.A.H. Johir, P. Loganathan, S. Vigneswaran, J. Kandasamy, Effectiveness of purolite A500PS and A520E ion exchange resins on the removal of nitrate and phosphate from synthetic water, Desalin. Water Treat. 47 (2012) 50–58.
[45] M. Rathod, K. Mody, S. Basha, Efficient removal of phosphate from aqueous solutions by red seaweed, *Kappaphycus alverezii*, J. Cleaner Prod. 84 (2014) 484–493.
[46] E. Chockalingam, S. Subramanian, Utility of *Eucalyptus tereticornis* (Smith) bark and *Desulfotomaculum nigrificans* for the remediation of acid mine drainage, Bioresour. Technol. 100 (2009) 615–621.
[47] F. Yao, J. Sun, C. Tang, W. Ni, Kinetics of ammonium, nitrate and phosphate uptake by candidate plants used in constructed wetlands, Procedia Environ. Sci. Part B 10 (2011) 1854–1861.
[48] Z. Wang, C.X. Liu, J. Dong, L. Liu, P.Y. Li, J.Y. Zheng, Screening of phosphate-removing filter media for use in constructed wetlands and their phosphorus removal capacities, Zhongguo Huanjing Kexue/China Environ. Sci. 33 (2013) 227–233.
[49] Z. Wang, J. Dong, L. Liu, G. Zhu, C. Liu, Screening of phosphate-removing substrates for use in constructed wetlands treating swine wastewater, Ecol. Eng. 54 (2013) 57–65.
[50] K. Sakadevan, H.J. Bavor, Phosphate adsorption characteristics of soils, slags and zeolite to be used as substrates in constructed wetland systems, Water Res. 32 (1998) 393–399.
[51] A. Drizo, C.A. Frost, J. Grace, K.A. Smith, Physico-chemical screening of phosphate-removing substrates for use in constructed wetland systems, Water Res. 33 (1999) 3595–3602.
[52] H. Yin, M. Kong, Simultaneous removal of ammonium and phosphate from eutrophic waters using natural calcium-rich attapulgite-based versatile adsorbent, Desalination 351 (2014) 128–137.
[53] S. Yagi, K. Fukushi, Removal of phosphate from solution by adsorption and precipitation of calcium phosphate onto monohydrocalcite, J. Colloid Interface Sci. 384 (2012) 128–136.
[54] K. Suzuki, Y. Tanaka, T. Osada, M. Waki, Removal of phosphate, magnesium and calcium from swine wastewater through crystallization enhanced by aeration, Water Res. 36 (2002) 2991–2998.
[55] Y. Sun, J. Lin, H. Huang, W. Zhang, D. Ma, Simultaneous removal of ammonium and phosphate from aqueous solution by calcium chloride-modified zeolite, Adv. Mater. Res. 356–360 (2012) 1581–1585.
[56] A. Pettersson, L.-E. Åmand, B.-M. Steenari, Leaching of ashes from co-combustion of sewage sludge and wood—Part I: Recovery of phosphorus, Biomass Bioenergy 32 (2008) 224–235.
[57] J.H. Li, G.H. Lv, W.B. Bai, Q. Liu, Y.C. Zhang, J.Q. Song, Modification and use of biochar from wheat straw (*Triticum aestivum* L.) for nitrate and phosphate

removal from water, Desalin. Water Treat. (2014) 1–13, doi: 10.1080/19443994.2014.994104.
[58] E. Lacasa, P. Cañizares, C. Sáez, F.J. Fernández, M.A. Rodrigo, Electrochemical phosphates removal using iron and aluminium electrodes, Chem. Eng. J. 172 (2011) 137–143.
[59] O.K. Borggaard, B. Raben-Lange, A.L. Gimsing, B.W. Strobel, Influence of humic substances on phosphate adsorption by aluminium and iron oxides, Geoderma 127 (2005) 270–279.
[60] J.P. Boisvert, T.C. To, A. Berrak, C. Jolicoeur, Phosphate adsorption in flocculation processes of aluminium sulphate and poly-aluminium-silicate-sulphate, Water Res. 31 (1997) 1939–1946.
[61] L. Zhu, R. Zhu, Simultaneous sorption of organic compounds and phosphate to inorganic-organic bentonites from water, Sep. Purif. Technol. 54 (2007) 71–76.
[62] G. Zelmanov, R. Semiat, The influence of competitive inorganic ions on phosphate removal from water by adsorption on iron (Fe^{+3}) oxide/hydroxide nanoparticles-based agglomerates, J. Water Process Eng. 5 (2015) 143–152.
[63] G. Zelmanov, R. Semiat, Phosphate removal from water and recovery using iron (Fe^{+3}) oxide/hydroxide nanoparticles-based agglomerates suspension (AggFe) as adsorbent, Environ. Eng. Manage. J. 10 (2011) 1923–1933.
[64] V. Masindi, M.W. Gitari, H. Tutu, M. De Beer, Application of magnesite–bentonite clay composite as an alternative technology for removal of arsenic from industrial effluents, Toxicol. Environ. Chem. 96 (2014) 1435–1451.
[65] V. Masindi, M.W. Gitari, H. Tutu, M. Debeer, Removal of boron from aqueous solution using magnesite and bentonite clay composite, Desalin. Water Treat. (2015) 1–11, doi: 10.1080/19443994.2015.1025849.
[66] V. Masindi, W.M. Gitari, K.G. Pindihama, Synthesis of cryptocrystalline magnesite/bentonite clay composite and its application for removal of phosphate from municipal wastewaters, Environ. Technol. (2015) 1–10.
[67] E. Iakovleva, E. Mäkilä, J. Salonen, M. Sitarz, S. Wang, M. Sillanpää, Acid mine drainage (AMD) treatment: Neutralization and toxic elements removal with unmodified and modified limestone, Ecol. Eng. 81 (2015) 30–40.
[68] A.B. Albadarin, C. Mangwandi, A.H. Al-Muhtaseb, G.M. Walker, S.J. Allen, M.N.M. Ahmad, Kinetic and thermodynamics of chromium ions adsorption onto low-cost dolomite adsorbent, Chem. Eng. J. 179 (2012) 193–202.
[69] D.L. Sparks, D.L. Sparks, Environmental Soil Chemistry, Academic Press, San Diego, CA, 2003.
[70] D.L. Sparks, Kinetics of Soil Chemical Processes, Academic Press, San Diego, CA, 1989.
[71] H.M. Selim, D.L. Sparks, Heavy Metals Release in Soils, Taylor & Francis, New York, NY, 2001.
[72] H.M. Selim, W.L. Kingery, Geochemical and Hydrological Reactivity of Heavy Metals in Soils, Taylor & Francis, UK, 2003.
[73] R. Rusmin, B. Sarkar, Y. Liu, S. McClure, R. Naidu, Structural evolution of chitosan–palygorskite composites and removal of aqueous lead by composite beads, Appl. Surf. Sci. 353 (2015) 363–375.
[74] L.A. Rodrigues, M.L.C.P. da Silva, Adsorption kinetic, thermodynamic and desorption studies of phosphate onto hydrous niobium oxide prepared by reverse microemulsion method, Adsorption 16 (2010) 173–181.
[75] S.Y. Yoon, C.G. Lee, J.A. Park, J.H. Kim, S.B. Kim, S.H. Lee, J.W. Choi, Kinetic, equilibrium and thermodynamic studies for phosphate adsorption to magnetic iron oxide nanoparticles, Chem. Eng. J. 236 (2014) 341–347.
[76] S. Mohamad, N.K.A. Bakar, A.R. Ishak, H. Surikumaran, K. Pandian, M. Raoov, N.N.M. Zain, K. Chandrasekaram, Removal of phosphate by paper mill sludge: Adsorption isotherm and kinetic study, Asian J. Chem. 26 (2014) 3545–3552.
[77] F.Z. Xie, G.J. Liu, F.C. Wu, G.L. Li, Y.R. Zhu, Removal of orthophosphate by adsorption onto activaed magnesium oxide in aqueous solution, Asian J. Chem. 24 (2012) 4238–4240.
[78] X. Song, Y. Pan, Q. Wu, Z. Cheng, W. Ma, Phosphate removal from aqueous solutions by adsorption using ferric sludge, Desalination 280 (2011) 384–390.
[79] J. Chen, Y. Cai, M. Clark, Y. Yu, Equilibrium and kinetic studies of phosphate removal from solution onto a hydrothermally modified oyster shell material, PLoS ONE 8(4) (2013) 1–10.
[80] M.W. Kamiyango, S.M.I. Sajidu, W.R.L. Masamba, Removal of phosphate ions from aqueous solutions using bauxite obtained from Mulanje, Malawi, Afr. J. Biotechnol. 10 (2011) 11972–11982.